Mechatronics 47 (2017) 37–48

Contents lists available at ScienceDirect

Mechatronics

journal homepage: www.elsevier.com/locate/mechatronics

Impedance control of series elastic actuators: Passivity and acceleration-based control☆

Andrea Calanca*, Riccardo Muradore, Paolo Fiorini

Department of Computer Science, University of Verona, Strada Le Grazie 15, 37134 Verona, Italy

ARTICLE INFO

Article history:
Received 6 April 2017
Revised 5 August 2017
Accepted 20 August 2017
Available online 8 September 2017

Keywords:
Series elastic actuators
Impedance control
Passivity
Acceleration-based control

ABSTRACT

Series elastic joints allow force and impedance controllers to be implemented on high torque and high power density motors. Several impedance controllers have been proposed whose stability is usually analyzed by means of passivity-based tools such as the *Z*-width characterization. This paper proposes an overview of existing impedance control solutions for series elastic joints and derives the passivity characterizations that are still missing in the literature, thus providing a complete and coherent overview of the existing solutions. Within this overview, we highlight the advantages of impedance control based on positive acceleration feedback showing improved stability robustness and impedance accuracy with respect to existing solutions. These advantages are theoretically motivated (considering ideal conditions) and experimentally validated.

1. Introduction

Series elastic actuators (SEA's) are an emerging technology to achieve high fidelity force control of high power density motors [1]. In fact, series compliance can dramatically improve explicit force control robustness [2,3]. Series elastic joints have been successfully applied to humanoid robots (e.g. NASA's Valkyrie [4], Virginia Tech's THOR [5] and IIT's COMAN [6]), quadrupeds (e.g. ETH's StarlETH [7]), modern rehabilitation and assistive robotics [8–11] and cooperative robots (e.g. RethinkRobotics Baxter [12]). Most of these applications are based on impedance control and need to deliver forces with a high level of safety and accuracy. While safety is a primary need for robots that interact with humans or with unstructured environments, the demand for high accuracy is increasing only recently. As an example, this requirement is pushed by novel haptic interfaces which have been proposed in the last years. Among others, Basafa et al. designed a haptic laparoscopic device with three degrees of freedom actuated by SEA's [13]; Zinn et al. proposed a haptic interface with large workspace based on the Distributed Macro-Mini concept where the macro actuation is given by SEA's [14]; Oblack et al. proposed a multi-purpose rehabilitation haptic device using series visco-elastic actuators [15]; Parietti et al. designed a haptic device with a series visco-elastic elements for very fine force rendering, in the range of the human sensory accuracy [16]. In these haptic devices, the choice of SEA's has been usually motivated by the decoupling effect of the series spring which allows to mask the motor inertia and allows the accurate rendering of even very low forces. Differently from traditional haptic interfaces, existing impedance controllers for SEA's make use of explicit force feedback, meaning that the force is explicitly measured and fed back to the control system. This is because implicit force control (where the force is delivered in open loop by controlling the motor current) cannot mask the motor inertia and cannot damp the series spring oscillations.

The control problem of physical interaction (with humans or with unstructured environments) involving explicit force feedback is considered a hard challenge in robotics. Most of the proposed solutions are based on the passivity interaction paradigm, which provides a high level of stability robustness [17]. In particular passivity of the controlled robot is a sufficient and necessary condition to guarantee a stable interaction with any passive environment [18] including humans who are usually assumed as passive systems [19]. Consequently several passivity-based control (PBC) algorithms have been proposed to shape the output impedance or the output force of SEA's. The first passive force controller for SEA's was proposed by Pratt and Williamson [1]. Their solution is based on acceleration feedback that forces the motor to have the same acceleration of the environment, thus compensating for load motion and leading to robust performance, i.e. predictable error dynamics. Quite surprising this important feature was not

☆ This paper was recommended for publication by Editor-in-Chief is Proof. Reza Moheimani.

* Corresponding author.
E-mail addresses: andrea.calanca@univr.it, andrea.calanca@gmail.com (A. Calanca), riccardo.muradore@univr.it (R. Muradore), paolo.fiorini@univr.it (P. Fiorini).

http://dx.doi.org/10.1016/j.mechatronics.2017.08.010
0957-4158/

explicitly highlighted neither in the original work nor in the following literature which has been focused more on stability robustness rather than performance robustness. Another investigation on PBC of SEA's has been conducted by Vallery et al. where a velocity sourced impedance control schema was considered [20]. They found out that "SEA cannot display a higher pure stiffness than the spring stiffness if passivity is desired". Thus the spring design cannot be arbitrarily compliant but must be tailored to the maximum desired stiffness leading to a trade-off between force control robustness (which requires compliance) and the maximum displayable stiffness.

One of the outcomes of the research described in this paper is to show that the same limitation highlighted by Vallery et al. holds for several existing control architectures: admittance control [21], impedance control [22] and parallel force-position control [23]. The admittance control architecture was proposed by Pratt et al. to reduce the force control bandwidth requirement in high impedance rendering [21]. We will show that even this algorithm cannot passively render a stiffness higher than the stiffness of the physical spring. A similar outcome emerges by analyzing the passive impedance control of the DLR lightweight arm where a parallel force-position architecture is implemented [23].

In conclusion, we will show that at the current state of the art *there exist no passive algorithms that allow to overcome the physical spring stiffness.* Further limitations arise when a virtual Voigt model impedance is desired, i.e. the parallel of a spring and a damper. For example an impedance controlled SEA with velocity controlled motor cannot passively display a pure Voigt model [24] and we will show that the same result holds for other control architectures. Thus, the *first contribution* of this work is to derive missing passivity conditions for existing impedance control architectures providing a coherent framework of passivity results.

The *second contribution* is a novel algorithm that allows in theory to passively overcome the physical spring stiffness and to passively display a pure Voigt model. This algorithm is inspired by the seminal work by Pratt and Williamson [1] who used load acceleration feedback to control the SEA output force and to cancel out the influence of load dynamics in force control. We will formally show that by taking advantage of load dynamics cancellation it is possible to passively render any passive impedance. The intuition behind this approach is that by exactly compensating for the load motion, load (or environment) uncertainties disappear. In particular we refer to (perfect) *load motion compensation* as the ability to move the motor *homokinetically* with the load or the environment. Thus load motion compensation is a way to obtain virtual backdrivability, i.e. to backdrive a non-backdrivable motor by control. Indeed, the force to accelerate the motor is transferred to the motor input by control and it is used to compensate for the motor inertia. In the past, the concept of load motion compensation has been already discussed in the force control literature and a generic framework of solutions is presented in [25]. However, the effects on impedance rendering and passivity have never been analyzed. Other examples of SEA's force control where the load dynamics is explicitly taken into account includes disturbance observer architectures [4,26–28], adaptive [29,30], robust [31] and sliding-mode [32] controllers. However, none of these works investigates the effect of load motion compensation on impedance rendering. We highlight that the terms "load" and "environment" can be often considered as equivalent: they both refer to the dynamics the SEA or the robot is in contact with. A typical case is physical human-robot interaction (pHRI) where the environment include or is identified with the human.

To address the issues described above, the paper is organized as follows. To introduce the reader, Section 2 summarizes existing impedance control algorithms for SEA's. Section 3 derives passivity conditions that are currently missing in the literature and provides a summary and easy-to-compare view of passivity results. Section 4 proposes a novel impedance control algorithm based on positive acceleration feedback. Section 5 experimentally compares the existing algorithms to our solution from the point of view of stability robustness and impedance accuracy. Finally, conclusions are drawn in Section 6.

2. Impedance control of series elastic actuators

Impedance control aims at shaping the dynamical relation between the actuator position (or velocity) and applied external forces. Impedance control can be implemented using an inner force loop and an outer position loop or using the dual configuration: an inner position loop and an outer force loop. The latter case is usually called admittance control. In both architectures the desired impedance/admittance is implemented in the outer loop while the inner loop must be fast enough to have negligible dynamics [33].

An impedance relation mapping the velocity $u \in L_{2e}$ into the force $y \in L_{2e}$ or equivalently an admittance relation mapping the force $u \in L_{2e}$ into the velocity $y \in L_{2e}$ is passive if there exists a constant β such that

$$\int_0^T u(t)y(t)dt \geq \beta, \ \forall u \in L_{2e}, \ \forall T \geq 0 \tag{1}$$

where $-\beta$ represents the initial system energy [18,34]. If we consider that (u, y) is a flow and effort pair we have that the system output energy will never be greater than its input energy, over an arbitrary observation time starting from t=0. The passive interaction paradigm is based on the assumption that the environment is a passive system and on the fact that negative feedback connection of passive systems is still passive, thus stable.

Passivity of impedance controllers depends on several factors: the control architecture, the inherent system dynamics and the desired impedance. In particular, given a control algorithm applied to a system, the set of impedance values that can be passively rendered is called Z-width [35]. Established results in PBC literature show that the controlled system dynamics cannot be too far from the inherent system dynamics [36]. In particular, Colgate et al. found that the virtual inertia of a current controlled motor cannot be reduced beyond one half of its physical inertia, using non-collocated proportional force feedback [17]. Similarly, Vallery et al. showed that the virtual stiffness of a SEA cannot be increased over the physical spring stiffness, considering a velocity sourced impedance control architecture [20].

Hereafter, several impedance control schemas are reported and their passivity is analyzed. We will start by introducing the common modeling and notation where linear and rotary quantities are regarded as equivalent.

2.1. Modeling

The following SEA model is considered

$$\tau_e = k(\theta - q) \tag{2}$$

$$J\ddot{\theta} = \tau_m - \tau_e \tag{3}$$

where τ_e is the spring force exerted on the environment (or torque in the case of a rotary joint), θ is the motor position, q is the joint position and τ_m is the (current-controlled) motor input force (or torque). Fig. 1 shows an equivalent linear representation of the system, which translates torques into forces and angular positions into linear positions. For the sake of generality, in this paper linear and angular quantities are used interchangeably. The SEA parameters are the spring stiffness k and the motor inertia J. In the existing SEA-passivity literature, the friction dynamics is usually neglected

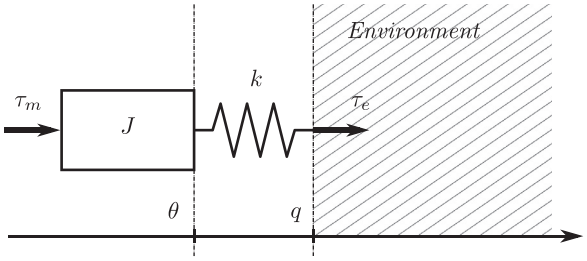

Fig. 1. A model of linear SEA interacting with an environment. Equivalent linear representation which translates torques into forces and angular positions into linear positions.

Table 1
Acronyms.

Acronyms	Meaning
SEA	Series elastic actuator
PBC	Passivity-based control
VM	Voigt model
∼VM	Approximated VM
BIC	Basic Impedance Control
VSIC	Velocity-Sourced Impedance Control
CAC	Collocated Admittance Control
CIC	Collocated Impedance Control
AB	Acceleration-based

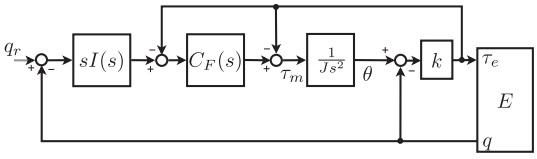

Fig. 2. Basic Impedance Control (BIC) which uses an outer non-collocated position loop to shape the impedance and an inner force control loop.

leading to a worst case condition: friction is dissipative and would help to meet passivity. The same choice is made here to ease the comparison with similar results in the literature while keeping the focus on the methodology.

2.2. Notation

Abbreviations and notations are listed in Table 1 and in the following points:

- The position and force control blocks are named $C_P(s)$ and $C_F(s)$, respectively.
- The impedance and admittance controllers are named $I(s)$ and $A(s)$, respectively.
- The position reference is q_r, which describes the equilibrium position of the desired impedance.
- The motor is modeled as a pure inertia $1/Js^2$ according to Eq. (3).
- The environment block is marked with the letter E and its input–output port is the pair $(\dot{q}, \tau_e)$. However, for ease of representation we considered the velocity integrator included in the environment block letting the position q be the environment output. Equivalent diagrams can be drawn considering $\dot{q}$ as output.

2.3. Impedance control architectures

Fig. 2 represents the basic arrangement for SEA impedance control. The inner force controller $C_F(s)$ is fed by an outer loop $I(s)$ that measures the load position and computes the force reference needed to obtain the desired impedance. For example, to render a

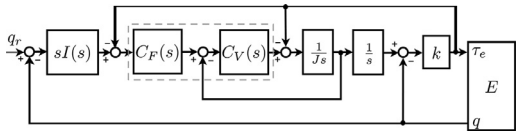

Fig. 3. Velocity-Sourced Impedance Control (VSIC) which uses an outer non-collocated position loop to shape the impedance and an inner force control loop with a nested velocity controller.

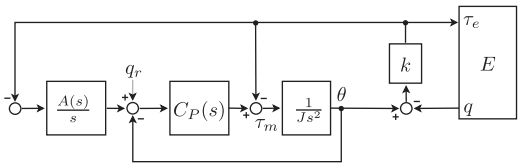

Fig. 4. Collocated Admittance Control (CAC). The position loop is closed on motor position θ (collocated) instead of on joint position q. The outer force loop shapes the impedance.

Voigt model (VM) impedance, the outer controller should be

$$sI(s) = d_d s + k_d \tag{4}$$

where k_d and d_d are the desired (positive and constant) stiffness and damping coefficients. The inner force loop may use a proportional-derivative action while the integral term is often avoided due to the passivity constraint [1]. We call this control architecture *Basic Impedance Control (BIC)*. Examples of this schema are in [22,37].

A common improvement of this schema is to add an inner motor velocity loop as shown in Fig. 3. This solution is often called "velocity-sourced" and helps to deal with friction in the transmission system [38,39]. Moreover, passivity allows for an integral action within the force loop [20,24]. We name this architecture *Velocity-Sourced Impedance Control (VSIC)*.

2.4. Collocated admittance architecture

Fig. 4 shows an admittance control approach with a motor position loop and an outer force feedback [21]. The position control loop on θ is *collocated* since the sensor is located on the same rigid body of the actuator (i.e. the encoder is on the rotor) [40]. A position control loop on q would be *non-collocated* and so more difficult to stabilize [41].

To render a visco-elastic impedance, the force controller computes the position reference as

$$\theta_{m,ref} = -\frac{A(s)}{s}\tau_e, \quad \frac{A(s)}{s} = \frac{1 - k_d/k}{k_d + s d_{dm}} \tag{5}$$

where k_d and d_{dm} are the desired stiffness and motor-level damping. Differently from classical admittance implementations [33], the position feedback is closed on the motor position instead of on the joint position, thus avoiding the non-collocation issue. For this reason we refer to this schema as *Collocated Admittance Control (CAC)*. Unfortunately this architecture cannot render a pure VM dynamics because the "virtual" damping cannot be rendered at joint-level (as it would require a non-collocated measure) but only at the motor side. In the ideal case of an infinitely fast inner control loop, the controlled actuator dynamics would be

$$d_{dm}\dot{\theta} + k_d q = -\tau_e, \tag{6}$$

meaning that the virtual damper can only act at the motor level and not at the joint level, thus resulting in an approximated Voigt model ($\sim VM$). On the contrary, the BIC and the VSIC architectures can display a joint level damping leading in ideal conditions (infinitely fast inner loops) to the VM dynamics

$$d_d\dot{q} + k_d q = -\tau_e. \tag{7}$$

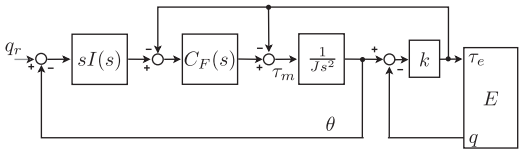

Fig. 5. Collocated Impedance Control (CIC). The architecture refers to its energetic interpretation as explained in [23]. The main difference with respect to BIC is that motor position is fed back instead of joint position.

2.5. Collocated Impedance Control

An alternative impedance architecture has been proposed for controlling the DLR lightweight arm [23]. This robot is modeled with flexible joints because of harmonic drive dynamics. From the modeling point of view a flexible joint is similar to a SEA except for the higher magnitude of elastic and damping parameters. Conceptually, the impedance controller of the DLR lightweight arm is based on a *Collocated Impedance Control (CIC)* architecture where an inner force loop is fed by an outer (collocated) motor position loop, as shown in Fig. 5. Similarly to the CAC case, collocation prevents virtual joint-level damping. In particular the outer controller can be computed as

$$sI(s) = d_{dm}s + k_{dm} \tag{8}$$

where d_{dm} is the desired motor-level damping and k_{dm} is the desired motor-level stiffness. By posing $k_{dm} = \frac{kk_d}{k-k_d}$, it is possible to set the desired joint-level stiffness leading, in ideal conditions, to the desired dynamics (6) where

$$k_d = \frac{kk_{dm}}{k + k_{dm}}. \tag{9}$$

Consequently, the physical spring limit $k_d = k$ can never be reached and can only be approached for very large (theoretically infinite) values of k_{dm}.

3. Passivity of existing solutions

This Section analyzes the passivity of existing impedance control architectures. In particular two kinds of desired impedance are considered: a pure spring dynamics ($sI(s) = k_d$) and a parallel spring-damper dynamics ($sI(s) = k_d + sd_d$). A compact overview of passivity results will then be summarized in Table 2.

Considering a linear time invariant system with impedance $Z(s)$ the passivity definition (1) is equivalent to the conditions (i) $Z(s)$ is stable and (ii) $\mathrm{Re}[Z(i\omega)] \geq 0\ \forall\omega \in \mathbb{R}^+$. In the following subsections, the conditions (i) and (ii) are derived for each control architecture, where $Z(s)$ is the impedance seen at the environment port $(\tau_e, \dot{q})$, i.e. $\tau_e = -Z(s)\dot{q}$ [18,34].

3.1. Basic Impedance Control (BIC)

For the BIC case a proportional-derivative force control law is considered

$$C_F(s) = P + sD \tag{10}$$

where P and D are positive constants. A pure integrator would violate the passivity of the inner force loop [1]. The impedance $Z(s)$ at the environment port $(\tau_e, \dot{q})$ can be computed as

$$-\tau_e = \frac{C_F(s)I(s) + Js}{C_F(s) + \frac{J}{k}s^2 + 1}\,\dot{q} \tag{11}$$

which is a stable transfer function. In the case $sI(s) = k_d$ one can compute

$$\mathrm{Re}[Z(i\omega)] = \frac{a(k_dD + d_dP) - PDk_d + \omega^2D^2d_d + \omega^2DJ}{a^2 + \omega^2D^2} \tag{12}$$

where $a = P + 1 - \omega^2\frac{J}{k} + i\omega D$. Solving for $\mathrm{Re}[Z(i\omega)] \geq 0$ [34] the following condition is derived:

$$k_d + \omega^2 J\left(1 - \frac{k_d}{k}\right) \geq 0. \tag{13}$$

Thus, passivity is equivalent to $k_d \leq k$, meaning that *a desired stiffness higher than the physical spring stiffness is not allowed by passivity*.

In the *VM* case, where $sI(s) = k_d + sd_d$ the condition (13) becomes

$$D\left[k_d + \omega^2 J\left(1 - \frac{k_d}{k}\right)\right] + d_d\left[P^2 + P - \omega^2(D^2 - \frac{JP}{k})\right] \geq 0 \tag{14}$$

which is implied by $k_d \leq k$ and $P \leq \frac{k}{J}D^2$. Since D is usually small to avoid noise amplification, the force proportional gain should be limited as well. This implies a bandwidth limitation for the inner force controlled system. Interestingly the bandwidth limit *depends on the actuator bandwidth*, i.e., the location of its mechanical resonance.

3.2. Velocity-Sourced Impedance Control (VSIC)

Sufficient passivity conditions for the VSIC schema have been reported in [20,24] considering $sI(s) = k_d$ and the following structure for the force and motor velocity controllers

$$C_F(s) = P_f + \frac{I_f}{s},\ C_V(s) = P_v + \frac{I_v}{s}. \tag{15}$$

Here a more general sufficient condition is reported, which is derived in Appendix A.1: passivity of the VSIC architecture is guaranteed if

$$k_d \leq \alpha k,\quad I_f + I_v\frac{P_f}{P_v} \leq \frac{P_fP_v}{J} \tag{16}$$

where $\alpha \geq 0$ depends on velocity and force gains

$$\alpha = \frac{I_v^2P_f}{I_v^2P_f + (I_vP_f + I_fP_v)k} < 1. \tag{17}$$

In conclusion

1. *passivity limits the maximum desired stiffness to (less than) the physical spring stiffness*,
2. given a sufficiently low value for $\frac{P_f}{P_v}$, no upper limit exists for the velocity and force proportional gains,
3. pure integrators are allowed both within the velocity and force loops, with limited integral gains. The smaller the integral gains the more k_d can approach k.

Finally, it has been shown that in the case $sI(s) = k_d + sd_d$ the VSIC architecture is not passive [24].

3.3. Collocated Admittance Control (CAC)

For the CAC case a passive position controller is considered

$$C_P(s) = P + sD \tag{18}$$

where P and D are positive constants. The impedance $Z(s)$ at the environment port is

$$-\tau_e = \frac{skI(s)(Js^2 + C_F(s))}{s[sI(s)(Js^2 + C_F(s)) - (k - k_d) - skI(s)]}\,\dot{q} \tag{19}$$

where $\frac{A(s)}{s}$ has been substituted with $\frac{1-k_d/k}{sI(s)}$. For the case $sI(s) = k_d$ passivity is equivalent to $k_d \leq k$, meaning again that *a desired stiffness higher than the physical spring stiffness is not allowed by passivity*. In the $\sim$*VM* case, where $sI(s) = k_d + sd_{dm}$, a sufficient and

Table 2
Passivity of existing impedance controllers.

	Control Architecture	Inner Control	Impedance	Z-Width / Passivity Constraints
BIC	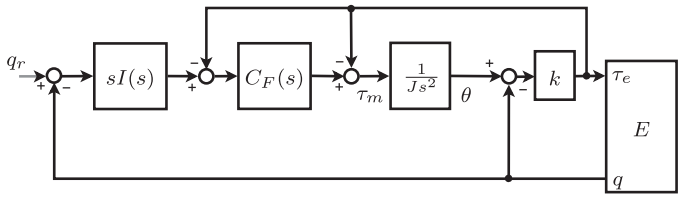	$C_F(s) = P + sD$	PS	passivity$\Longleftrightarrow k_d \leq k$
			VM	passivity$\Longleftarrow k_d \leq k$, $\frac{P}{D} \leq D\frac{k}{J}$ bandwidth limitations for the force controlled system, depending on the actuator bandwidth.
			—	—
VSIC	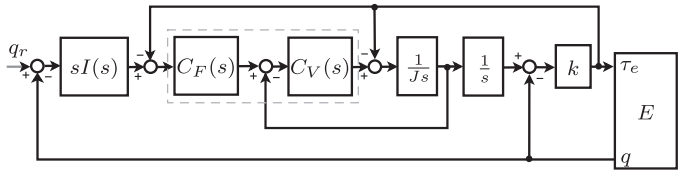	$C_F(s) = P_f + \frac{I_f}{s}$ $C_V(s) = P_v + \frac{I_v}{s}$	PS	passivity$\Longleftarrow k_d \leq \alpha k < k$, $I_f + I_v\frac{P_f}{P_v} \leq \frac{P_f P_v}{J}$ pure integrators are allowed with limited integral gains [20]
			VM	not passive [24]
			—	—
CAC	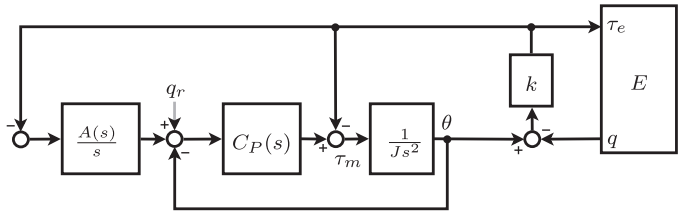	$C_P(s) = P + sD$	PS	passivity$\Longleftrightarrow k_d \leq k$
			VM	not allowed
			$\sim VM$	passivity$\Longleftrightarrow$ $d_{dm}\left[\frac{P}{D} - \frac{d_{dm}}{J\bar{k}} - \frac{D}{J}\right] < k_d \leq k$ a lower limit for the desired stiffness may arise depending on position bandwidth, motor inertia and desired damping
CIC	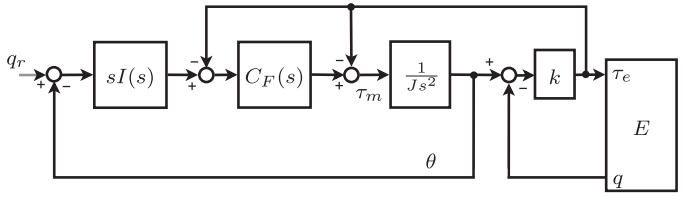	$C_F(s) = P + sD$	PS	passivity$\Longleftrightarrow k_d \leq k$
			VM	not allowed
			$\sim VM$	passivity$\Longleftrightarrow k_d \leq k$

Notation: I, P, D are positive integral, proportional and derivative gains. Desired impedance dynamics: pure spring (PS), parallel spring and damping (VM, see (7)) and approximate VM ($\sim VM$, see (6)), respectively.

Note: The condition $k_d \leq k$ holds for all existing control architectures, meaning that *the maximum desired stiffness is upper limited by the physical spring stiffness.*

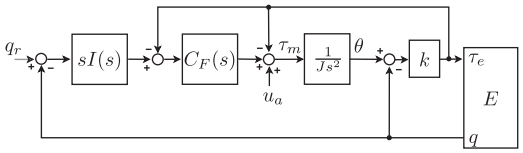

Fig. 6. Impedance control based on acceleration feedback. This architecture is identical to the BIC scheme in Fig. 2 except from the additional term u_a.

necessary condition for passivity is

$$d_{dm}\left[\frac{P}{D}-\frac{1}{J}\left(\frac{d_{dm}}{\bar{k}}+D\right)\right]<k_d\leq k \tag{20}$$

where $\bar{k}=1-\frac{k_d}{k}$. This means that the desired stiffness may be bounded from below. Interestingly, sufficient conditions for passivity are

$$k_d\leq k,\quad \frac{P}{D}<\frac{k_d}{d_{dm}} \tag{21}$$

meaning that the position gain P is upper limited. This implies bandwidth limitations for the position controlled sub-system *depending on the desired impedance*. Condition (21) also indicates that a high derivative gain D helps to meet passivity. The proofs of (20) and (21) are missed in the literature and are reported here in Appendix A.2.

3.4. Collocated Impedance Control (CIC)

Passivity of the CIC architecture has been already investigated considering an energy shaping interpretation [42]. In particular, the motor kinetic energy is shaped via inner force feedback and the potential energy via outer position feedback, then, the total energy function is used as a candidate Lyapunov function. Considering our modeling, passivity is equivalent to positiveness of P, D, k_{dm} and d_{dm}. According to (9) setting a motor-level stiffness implies that *the maximum desired stiffness cannot overcome the physical spring stiffness*, i.e., $k_d \leq k$. Details are reported in Appendix A.3.

4. Acceleration-based impedance control

The previous Section showed that all the existing implementations of impedance and admittance control are constrained to the same passivity limitation, i.e. *it is not possible to overcome the stiffness of the physical spring.* In addition, it is not always possible to render an exact VM impedance due to passivity constraints and/or architecture limitations. The only architecture that allows the passive rendering of an exact VM impedance is the BIC algorithm, if the inequality (14) is verified.

This Section proposes an impedance controller based on positive acceleration feedback, which allows to overcome the passivity limitations of existing architectures.[1] This algorithm is designed considering the BIC architecture and adding the following term to the motor input torque

$$u_a(t)=\frac{J}{k}\ddot{\tau}_d(t)+\tau_d(t)+J\ddot{q}(t) \tag{22}$$

where $\tau_d = sI(s)(q_r - q)$ is the output of the outer impedance controller, as shown in Fig. 6. The feed-forward term $\tau_d(t)$ in (22) accounts for the desired force reference and delivers it directly on the motor input. The term $\frac{J}{k}\ddot{\tau}_d(t)$ considers the motor acceleration needed to compress the spring, to reach perfect torque tracking. In fact, the SEA model (2)–(3) can be rearranged as

$$J\ddot{q}+\frac{J}{k}\ddot{\tau}_e+\tau_e=\tau_m \tag{23}$$

where the term $\frac{J}{k}\ddot{\tau}_e$ accounts for motor acceleration to compress the spring and is peculiar of series elastic systems. Finally, the term $J\ddot{q}(t)$ in (22) provides the torque to accelerate the motor homokinetically with the environment leading to compensate for the influence of the environment dynamics. We highlight that some caution is needed when implementing the term $J\ddot{q}(t)$: overestimation of J leads to feedback inversion and to loose passivity. In real implementation a slight underestimation of J is suggested to avoid this issue as discussed later in this section. By considering u_a it is possible to write

$$-\tau_e=\frac{C_F(s)I(s)+Js^2}{C_F(s)+\frac{J}{k}s^2+1}\,\dot{q}-\frac{1}{C_F(s)+\frac{J}{k}s^2+1}\,u_a. \tag{24}$$

Then, the overall impedance seen at the environment port can be computed considering the Laplace transform of (22)

$$u_a=\left(\frac{J}{k}s^2+1\right)I(s)\dot{q}+Js\dot{q} \tag{25}$$

and by substituting (25) in (24) one ends up with

$$-\tau_e=I(s)\dot{q} \tag{26}$$

meaning that *the shaped actuator impedance is equal to the desired impedance*. This leads to a novel result: *the passive rendering of any passive impedance*, which is formally stated in the following Proposition.

Proposition 4.1. *Given the series elastic actuator (2)–(3) and the control law*

$$\tau_m=-C_F(s)(s\theta I(s)+\tau_e)+u_a \tag{27}$$

$$u_a=\left[\left(s^2\frac{J}{k}+1\right)sI(s)+s^2J\right]q \tag{28}$$

with $I(s)$ passive and $C_F(s)$ stable, then the controlled system is passive at the environment port $(\tau_e,\ \dot{q})$.

Hence, *the knowledge of $\ddot{q}$ allows to overcome the passivity constraint of all the existing architectures*. In fact, the proposed control law allows, theoretically, to render unlimited desired stiffness and unlimited desired damping. Moreover, Eq. (26) states that, unlike other architectures, the rendered impedance is equal to the desired impedance over the entire frequency spectrum. Of course such theoretical expectations are too optimistic when compared to practical implementations where the acceleration signal is usually noisy and with limited bandwidth. In addition, it is known that "discrete control, time delays, actuator and sensor limitations and unmodeled dynamics can compromise passivity, making the implementation of passive control on real systems extraordinarily challenging" [36]. However, Proposition 4.1 provides a theoretical insight to motivate the use of BIC endorsed with positive acceleration feedback and the next Section shows experimentally that such architecture outperforms the existing solutions in terms of both impedance accuracy and robustness. Before to proceed with the experimental part, we highlight a practical issue with the acceleration-based (AB) law (27) and (28). It has been reported in the literature that feeding back the acceleration term $J\ddot{q}(t)$ may lead to feedback inversion and instability in the case the parameter J is over-estimated [1,25]. As mentioned before the term $J\ddot{q}(t)$ provides the torque to accelerate the motor homokinetically with the environment, however, if the parameter J is over-estimated the motor accelerates more than the environment possibly leading to instability. For this reason a

[1] A preliminary version of this Section appeared as abstract in the International Symposium on Wearable Robotics, 18–21 October, 2016. La Granja, Segovia, Spain [43].

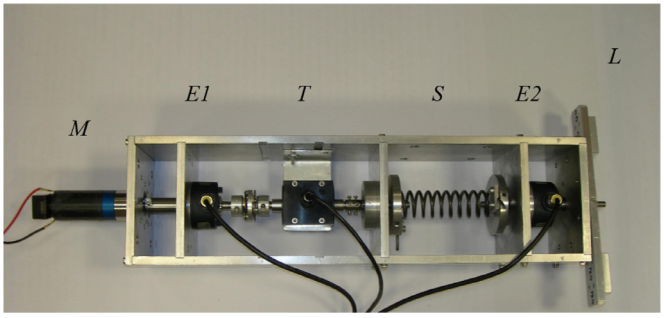

Fig. 7. The SEA prototype used as testbed: M is the motor, T is a torque sensor (used for identification), S is a torsional spring and the angular quantities θ and q are measured by encoders E_1 and E_2, respectively. L is a metal frame used as inertial load in uncoupled conditions.

reduction gain $0 < k_J < 1$ can be used in practical implementation of (27) and (28) leading to substitute (28) with

$$u_a = \left[\left(s^2\frac{J}{k}+1\right)sI(s) + s^2 k_J J\right]q. \tag{29}$$

Fortunately, passivity of control law (27)–(29) is still verified, as stated in the following proposition where a proportional-derivative form for the controller $C_F(s)$ is assumed. Within the proof one can observe that – differently from Proposition 4.1 – a small k_J causes the rendered impedance to deviate from desired impedance. Thus, the gain k_J should be tuned as high as possible while allowing stable acceleration feedback.

Proposition 4.2. *Given the series elastic actuator (2)–(3) and the control law (27)–(29) with $k_J < 1$, $I(s)$ passive and $C_F(s)$ as in (10), then the controlled system is passive at the environment port $(\tau_e, \dot{q})$.*

Proof. By substituting (29) in (24) the following impedance relation can be found:

$$-\tau_e = \left[I(s) + \frac{(1-k_J)Js^2}{C_F(s) + \frac{J}{k}s^2 + 1}\right]\dot{q}. \tag{30}$$

As the parallel interconnection of passive system is still passive and $I(s)$ is passive we just need to verify passivity of the remaining term

$$I_e(s) = \frac{(1-k_J)Js^2}{P + sD + \frac{J}{k}s^2 + 1} \tag{31}$$

which represents the deviation from the desired impedance $I(s)$. It can be verified that $Re[I_e(i\omega)] > 0$ is equivalent to $\omega^2 D > 0$ which holds because $D > 0$. □

5. Experimental validation

This Section presents an experimental comparison of the described control architectures in terms of experimental coupled stability and impedance accuracy. Experiments are conducted in a physical human-robot interaction scenario where a human can exert forces on the impedance controlled joint of the SEA prototype shown in Fig. 7. The prototype is composed of a geared DC motor M connected in series to a spring S and then to a metal frame L. Two optical encoders ($E1$ and $E2$) are used to measure the motor and the load positions (with a resolution of 0.018 degrees) while the torque is measured using spring displacement. The torque sensor T is used only for identification purposes. Velocities are obtained by measuring pulse inter-periods (using hardware timers available on the encoder electronics) which give a better approximation than using finite differences, as shown in Fig. 8. Accelerations are obtained by numerical differentiation of velocities with

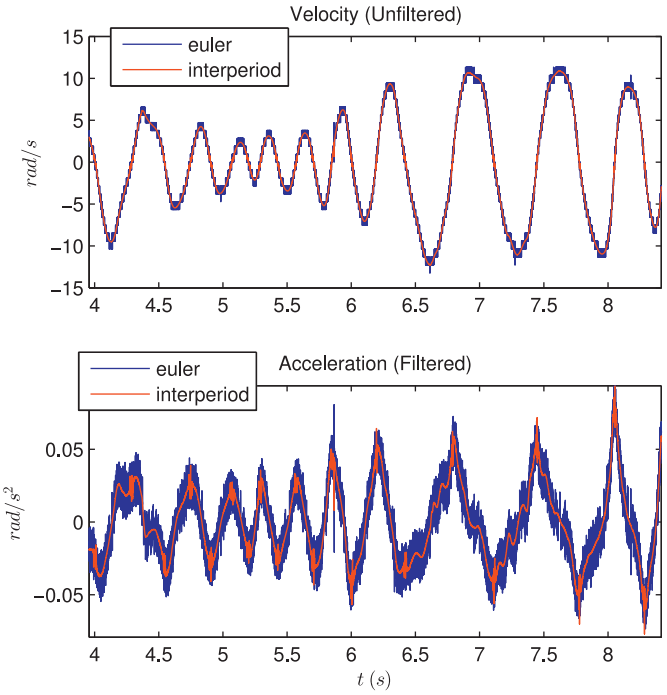

Fig. 8. Upper plot: comparison between velocity by numerical position differentiation (blue) and inter-period measurements (red). Lower plot: comparison between acceleration estimations. (For interpretation of the references to color in this figure legend, the reader is referred to the web version of this article.)

Table 3
System parameters of the SEA testbed.

Parameter	Symbol	Value
Spring stiffness	k	2.49 N m/rad
Torque constant	k_t	2.29 N m/A
Motor inertia	J	0.0208 kg/m^2
Load inertia	J_{load}	0.0021 kg/m^2

Table 4
Control tuning.

		Gain	Tuning
BIC	C_F	P	80
		D	1.5
VSIC	C_V	P_v	1
		I_v	0.45
	C_F	P_f	100
		I_f	50
CAC	C_P	P	100
		D	1
CIC	C_F	P	50
		D	1
AB	C_F	P	80
		D	1.5
		k_J	0.8

an output stage filter at 20Hz. System parameters have been estimated using a procedure similar to the one described in [44] and are listed in Table 3.

The control system runs on a standard PC equipped with a quad-core processor running a real-time process with kernel-like priority. The control process runs at 3kHz and communicates with the motor drive and the sensor electronics via Ethercat protocol at the same rate. Position and force controllers have been tuned in order to achieve the highest performance (maximum bandwidth and minimum static error) within the allowed passivity constraint and without introducing noise into the system. Table 4

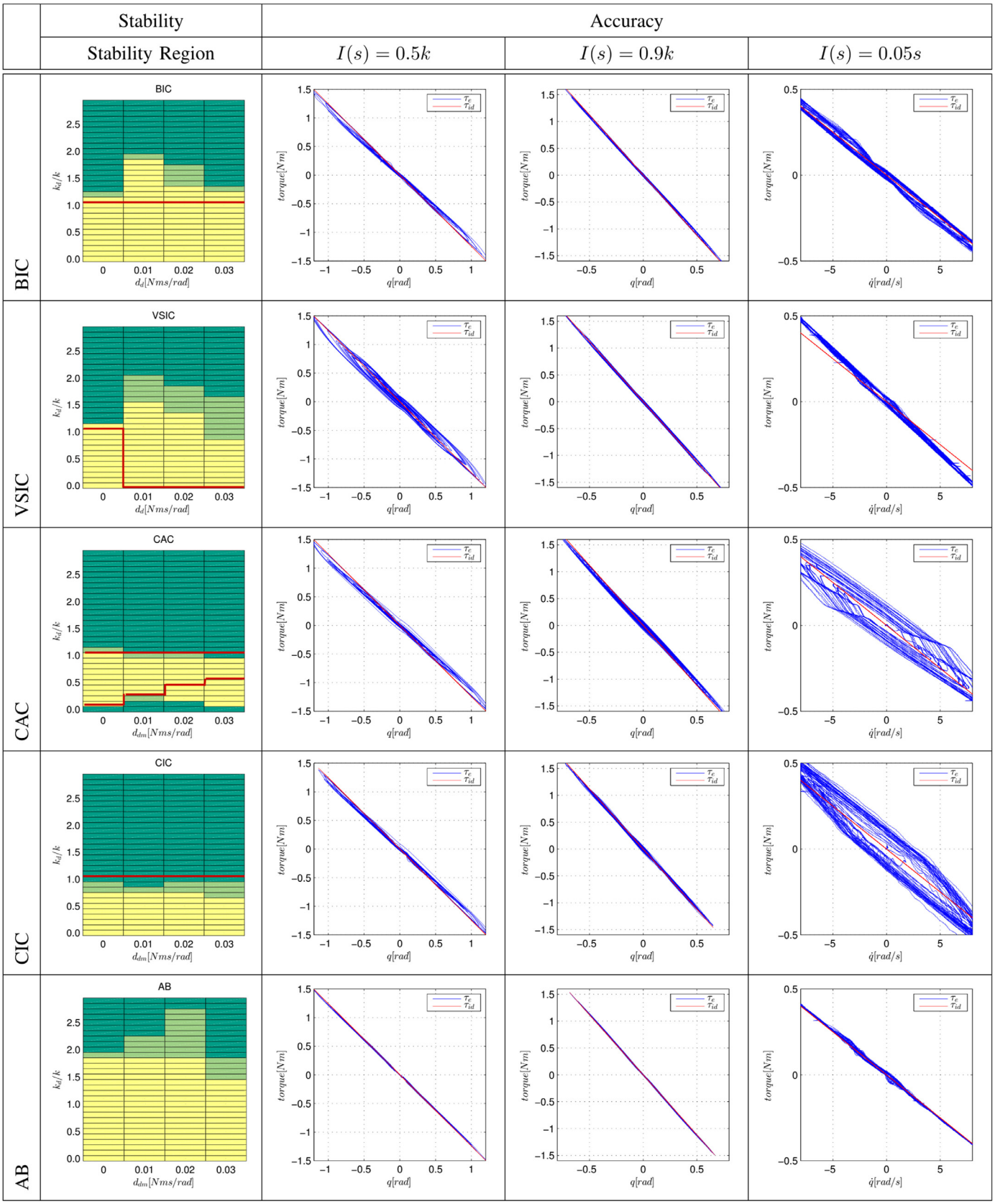

Fig. 9. Experimental results. Column 1 (from left): experimental stability region, yellow cells represent stable responses while light and dark green cells represent critical and unstable responses; red lines represents the theoretical passivity constraints. Columns 2–4: impedance accuracy of pure stiffness (cols 2 and 3) and pure damping (col 4) desired impedances (red lines). (For interpretation of the references to color in this figure legend, the reader is referred to the web version of this article.)

shows the controllers gains used in the experiments including the proposed acceleration-based (AB) algorithm, which uses a proportional derivative force controller as in (10). BIC and CIC algorithms have been tuned satisfying conditions (14) and (20) which allow for passive rendering of a *VM* and $\sim VM$ impedance, respectively. In particular for the BIC case one has $P = 80 \leq \frac{k}{J}D^2 = 269.3$ which satisfies condition (14). The control algorithms have been implemented in C++ and are open-source released within the Series Elastic Library (http://metropolis.scienze.univr.it/altair/selib/).

5.1. Experiments to assess the stability region

The stability regions are evaluated in terms of maximum desired damping and stiffness that can be stably rendered. During experiments the system is manually perturbed with a torque of about 0.5*Nm* and the observed behavior is classified as stable, critical or unstable. *Critical* means that unexpected dynamics is observed, including undesired high frequency vibrations/chattering and undamped low frequency oscillations. *Unstable* means that divergence is observed. For each algorithm, a desired stiffness in the range $[k, 3k]$ and a desired damping in the range $[0, 0.03]\frac{Nms}{rad}$ have been tested. Of course in the collocated cases (CAC and CIC) the desired damping is considered at motor-level only, i.e., d_{dm} instead of d_d. The experiments have been repeated several times until the outcomes have been judged unanimously by three different subjects experts in control. Experimental results are reported in the first column of Fig. 9 where each cell in the grid-plots represents the outcome of an experiment. Yellow cells represent experimentally stable responses while light and dark green cells represent critical and unstable responses, respectively. As a first observation we highlight that the stability region of the AB architecture is larger than others according to the theoretical insight reported in Section 4. A second observation is that for BIC, VSIC and CAC algorithms the experimental stability agrees with the passivity constraints derived in Section 3, represented with red lines. In fact, a passive system is also stable. The stability region of the CIC algorithm is slightly smaller than the theoretical *Z*-width. This is because the limit $k_d = k$ cannot be reached unless $k_{dm} \to \infty$ which is not realizable in practice. Of course stability can be observed even outside of the passivity region. In particular, within the described experimental conditions

1. the VSIC architecture can stably render a *VM* impedance,
2. for high desired damping values (d_{dm}), the CAC architecture is stable even below the lower bound on k_d given by passivity.

It is worth highlighting that because of missing passivity, these observed stabilities are strongly related to the specific load condition. For instance, we observed the VSIC algorithm cannot any more stably render a *VM* impedance if we arrange small load inertias.

Regarding the AB controller, we found instabilities only for $k_d > 2k$ leading to a stability region twice larger than other architectures. Displaying a wider stability region agrees with theoretical results, however, the stability region is not infinitely large as expected from the theoretical analysis. This is possibly due to existing unmodeled effects in the hardware (e.g. current loop dynamics, acceleration sensor bandwidth) and in the software implementations (e.g. digital delay, numerical approximation) which prevent to display arbitrarily large impedances. In other words, Proposition 4.2 assumes no current dynamic and ideal acceleration measurements (zero-latency, infinite bandwidth) which cannot be found in practice. Experimentally, this translates in a wider but still limited stability region. We highlight that a similar discrepancy can be found in the practical implementation of almost all passive controllers. Let us consider in example proportional-derivative position or force controllers which are commonly assumed as passive

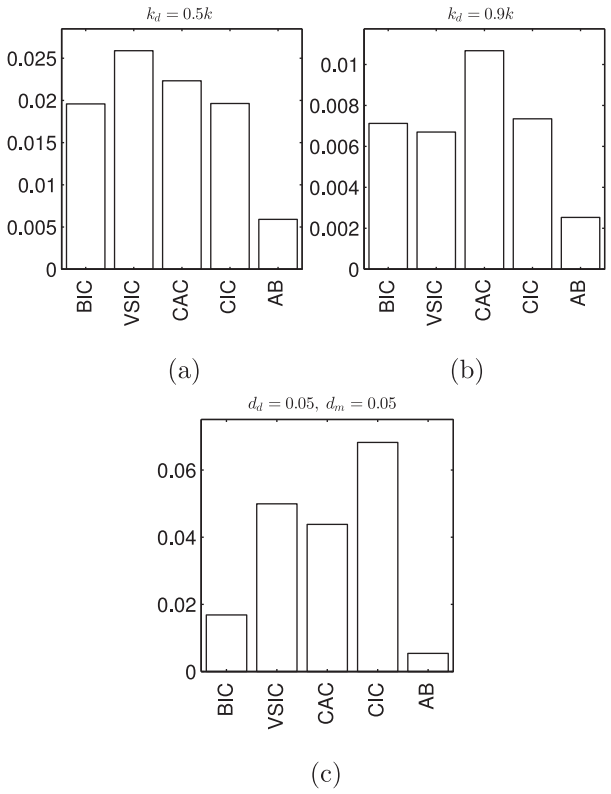

Fig. 10. Accuracy comparison terms of average impedance distance. Plot (a) compares accuracy considering a pure spring impedance with $k_d = 0.5k$, plot (b) considers a pure spring impedance with $k_d = 0.9k$ and plot (c) a pure damping impedance with $d_d = 0.05\frac{Nms}{rad}$.

in continuous domain analyses. In both cases practical implementations easily show instability when the proportional or derivative gain exceed certain thresholds. This is again because of digital delay and neglected current and sensor dynamics. A more accurate analysis of these phenomena should account for discrete time and sampled data. In the case of algorithm (27)–(29) such analysis deserves a separate study and will be matter of future research.

5.2. Experiments to assess the impedance accuracy

The accuracy of different architectures is evaluated as follows. The series elastic joint is controlled considering two kinds of desired impedance: (a) pure spring impedance and (b) pure damping impedance. In the case (a), the human starts holding the frame L by hand and pushes it to reach an angular displacement of about 45°. Then, the human suddenly releases the frame which comes back to its rest position accordingly to the desired impedance dynamics. In the case (b) the human rotates the actuator frame in both directions and at different speeds. The duration of each experiment is 15 s. Results are shown in Fig. 9 considering force-displacement plots (pure stiffness impedances in columns 2 and 3) or force-velocity plots (pure damping impedance in column 4). The desired impedance is represented by a red line. The lower the distance from the red line, the better the impedance accuracy is. In particular the impedance error is computed for each sample (q, τ_e) as the minimum distance from the red line. In the case (b) samples $(\dot{q}, \tau_e)$ are considered. Average errors are summarized in Fig. 10 showing that the AB controller is on average three to four times more accurate than the other architectures. The other architectures behave similarly except for the case of pure damping impedance where

1. the VSIC architecture shows a biased damping due to the inner motor velocity dynamics,
2. the CAC and CIC architectures show lower accuracy because of their collocated nature which does not allow to display an exact *VM*.

A further observation is that when k_d approaches k (in pure stiffness impedance), the accuracy of each architecture improves. This is because when k_d is close to k the desired impedance is similar to the inherent mechanical impedance. In other words, the more k_d approaches k, the less the motor needs to move; in the limit case $k_d = k$ the motor just needs to stand still. For a similar reason, the accuracy of damping rendering is lower than stiffness rendering. In fact, the inherent actuator dynamics is spring-like and the controllers need to transform it into a damping-like impedance.

As a final remark, we observe that - according to the theoretical insights in Section 4 - the AB algorithm shows experimental evidence of significantly higher stability and improved accuracy with respect to other solutions. *The experimental stability region is almost doubled in size while the accuracy is more than tripled.*

6. Conclusion

This paper reported our effort to motivate and foster positive acceleration feedback in impedance control. Improved stability and superior accuracy with respect to existing solutions has been experimentally shown and theoretically motivated. Beside this methodology, this paper derived missing passivity results for SEA impedance control solutions showing a common Z-width limitation (e.g. the physical spring stiffness limit) that holds for all architectures except for acceleration-based control. Also we derived algorithm-specific limitations, summarized in Table 2, providing a comprehensive and coherent comparison of controller passivity. Finally, the passivity results have been validated experimentally in terms of coupled stability showing agreement with theoretical expectations.

Appendix A

A1. Deriving condition (16)

According to Eq. (9) in [20] the real part of impedance at the environment port is proportional to

$$\mathrm{Re}[Z(i\omega)] \propto \omega^4(d_6\omega^2 + d_4)$$

with

$$d_4 = k[I_v^2 P_f(k - k_d) - akk_d] \tag{A.1}$$

$$d_6 = k[(P_v^2 P_f - aJ)(k - k_d) + P_v k] \tag{A.2}$$

where $a = I_v P_f + I_f P_v$. Sufficient and necessary conditions for stability are

$$d_4 \geq 0,\ d_6 \geq 0. \tag{A.3}$$

The condition $d_4 \geq 0$ is equivalent to

$$k_d \leq k\frac{I_v^2 P_f}{I_v^2 P_f + ak} \tag{A.4}$$

which implies $k_d < k$. Finally a sufficient condition for $d_6 \geq 0$ is $P_v^2 P_f - aJ \geq 0$ which results in $I_f + I_v\frac{P_f}{P_v} \leq \frac{P_f P_v}{J}$. Condition (16) is then sufficient for passivity.

A2. Deriving condition (21)

Substituting (18) and (4) in (19) one gets

$$Z(s) = \frac{num(s)}{den(s)} = \frac{\alpha s^3 + \beta s^2 + \gamma s + \delta}{as^4 + bs^3 + cs^2 + ds} \tag{A.5}$$

where

$$\alpha = Jd_d,\ \beta = Jk_d + d_{dm}D,\ \gamma = d_{dm}P + k_d D,\ \delta = k_d P, \tag{A.6}$$

$$a = \frac{\alpha}{k},\ b = \frac{\beta}{k},\ c = \frac{\gamma}{k} + \frac{\bar{k}}{k}D + d_{dm},\ d = \frac{\delta}{k} + \frac{\bar{k}}{k}P + k_d, \tag{A.7}$$

with $\bar{k} = 1 - \frac{k_d}{k}$. The real part of $Z(i\omega)$ is proportional to $Re[num(i\omega)]Re[den(i\omega)] + Im[num(i\omega)]Im[den(i\omega)]$, i.e.

$$Re[Z(i\omega)] \propto \omega^2[(\bar{D}\beta - \bar{P}\alpha)\omega^2 + (\bar{P}\gamma - \bar{D}\delta)] \tag{A.8}$$

where $\bar{D} = (d_{dm} + \bar{k}D)$ and $\bar{P} = (k_d + \bar{k}P)$. Condition $Re[Z(i\omega)] \geq 0$ is equivalent to

$$\bar{D}\beta - \bar{P}\alpha \geq 0 \wedge \bar{P}\gamma - \bar{D}\delta \geq 0. \tag{A.9}$$

The inequality $\bar{D}\beta - \bar{P}\alpha \geq 0$ leads to

$$\frac{D}{P} > \frac{d_{dm}}{k_d} - \frac{d_{dm}^2 Dk + D^2 d_{dm}(k - k_d)}{Pk_d J(k - k_d)} \tag{A.10}$$

which is implied by $k_d \leq k$, $\frac{D}{P} > \frac{d_{dm}}{k_d}$. Also (A.10) can be further arranged as

$$k_d > d_{dm}\left[\frac{P}{D} - \frac{1}{J}\left(\frac{d_{dm}}{\bar{k}} + D\right)\right] \tag{A.11}$$

which may lead to a lower bound for the desired stiffness. The condition $\bar{P}\gamma - \bar{D}\delta \geq 0$ leads to

$$k_d^2 D + \bar{k}P^2 d_{dm} > 0 \tag{A.12}$$

which is implied by $k_d < k$. Sufficient and necessary conditions for passivity are (A.10) and (A.12) whereas (21) represents only sufficient conditions. In the case of a pure spring impedance ($d_{dm} = 0$) the sufficient and necessary conditions (A.10) and (A.12) reduce to $k_d < k$.

A3. Passivity of Collocated Impedance Control

The idea underlying the CIC architecture is to shape the kinetic energy via force feedback and the potential energy via position feedback. Translating the multidimensional and non-linear controller in [23] to our notation, the force loop is implemented as

$$\tau_m = JJ_d^{-1}u + (1 - JJ_d^{-1})\left(\tau_e + \frac{\hat{d}}{k}\dot{\tau}_e\right) \tag{A.13}$$

where $J_d < J$ is a desired inertia, $\hat{d} > 0$ is a damping parameter and u is an auxiliary input coming from the outer position loop. When we apply (A.13) in (2) and (3) the following passive dynamics (from τ_e to $\dot{q}$) is obtained:

$$J_d\ddot{\theta} = u - \tau_e \tag{A.14}$$

and the parameter J_d can be used to shape the kinetic energy. To shape the potential energy a collocated position feedback is used

$$u = -\hat{k}_{dm}(\theta - q_r) - \hat{d}_{dm}\dot{\theta} \tag{A.15}$$

where $\hat{k}_{dm}$, $\hat{d}_{dm} > 0$, and θ_r is the desired link position. With this controller the dynamics of (A.14) becomes

$$J_d\ddot{\theta} + \hat{k}_{dm}(\theta - q_r) + \hat{d}_{dm}\dot{\theta} = -\tau_e \tag{A.16}$$

where the control potential energy is shaped via $\hat{k}_{dm}$ and the dissipation via $\hat{d}_{dm}$. Thus, the joint level stiffness is given by the series of k and $JJ_d^{-1}\hat{k}_{dm}$ and the motor level damping is $\hat{d}_{dm}$. From the architectural point of view this energetic interpretation resembles an impedance schema but with collocated position feedback where force gains are given by $P = (1 - JJ_d^{-1})$, $D = (1 - JJ_d^{-1})\frac{\hat{d}}{\hat{k}}$ and position gains by $k_{dm} = JJ_d^{-1}\hat{k}_{dm}$, $d_{dm} = JJ_d^{-1}\hat{d}_{dm}$. By choosing the total system energy as Lyapunov function candidate passivity is ensured by positiveness of P, D, k_{dm} and d_{dm} [23].

References

[1] Pratt GA, Williamson M. Series elastic actuators. In: Proceedings of international conference on intelligent robots and systems, 1. IEEE; 1995. p. 399–406. http://ieeexplore.ieee.org/xpls/abs_all.jsp?arnumber=525827.

[2] Whitney D. Force feedback control of manipulator fine motions. Trans ASME, J Dyn Syst Meas Control 1977;99(2):91–7. doi:10.1115/1.3427095.

[3] Calanca A, Fiorini P. On the role of compliance in force control. In: Menegatti E, Michael N, Berns K, Yamaguchi H, editors. Proceedings of international conference on intelligent autonomous systems, IAS-13. Padova, Italy: Springer International Publishing; 2014. doi: 10.1007/978-3-319-08338-4_90.

[4] Paine N, Mehling JS, Holley J, Radford NA, Johnson G, Fok CL, Sentis L. Actuator control for the NASA-JSC valkyrie humanoid robot: a decoupled dynamics approach for torque control of series elastic robots. J Field Rob 2015;32(3):378–96.

[5] Knabe C, Lee B, Orekhov V, Hong D. Design of a compact, lightweight, electromechanical linear series elastic actuator. In: Proceedings of ASME international design engineering technical conferences; 2014. p. 1–8. doi:10.1115/DETC2014-35096. ISBN 978-0-7918-4637-7.

[6] Ajoudani A, Lee J, Rocchi A, Ferrati M, Hoffman EM, Settimi A, et al. A manipulation framework for compliant humanoid COMAN: application to a valve turning task. In: Proceedings of IEEE-RAS international conference on humanoid robots; 2015. p. 664–70. doi:10.1109/HUMANOIDS.2014.7041434. ISBN 9781479971749; 2015-Febru.

[7] Remy CD, Siegwart R, Gehring C, Bloesch M, Hoepflinger MA, Hutter M. StarlETH: a compliant quadrupedal robot for fast, efficient, and versatile locomotion. In: Proceedings of 15th international conference on climbing and walking robot, CLAWAR 2012; 2012. p. 1–8. doi:10.1142/9789814415958_0062.

[8] Baser O, Kizilhan H, Kilic E. Mechanical design of a biomimetic compliant lower limb exoskeleton (BioComEx). Proceedings - 2016 International Conference on Autonomous Robot Systems and Competitions, ICARSC 2016. 2016. pp. 60–65, doi:10.1109/ICARSC.2016.51.

[9] Wang S, Wang L, Meijneke C, Van Asseldonk E, Hoellinger T, Cheron G, et al. Design and control of the MINDWALKER exoskeleton. IEEE Trans Neural Syst Rehabil Eng 2015;23(2):277–86. doi:10.1109/TNSRE.2014.2365697.

[10] Kwa HK, Noorden JH, Missel M, Craig T, Pratt JE, Neuhaus PD. Development of the IHMC mobility assist exoskeleton. In: Proceedings of IEEE international conference on robotics and automation; 2009. p. 2556–62. doi:10.1109/ROBOT.2009.5152394. ISBN 9781424427895.

[11] Ekkelenkamp R, Veneman J, van der Kooij H. LOPES: selective control of gait functions during the gait rehabilitation of CVA patients. In: Proceedings of 9th international conference on rehabilitation robotics, ICORR 2005; 2005. p. 361–4. doi:10.1109/ICORR.2005.1501120.

[12] Liang P, Yang C, Wang N, Li Z, Li R, Burdet E. Implementation and test of human-operated and human-like adaptive impedance controls on Baxter robot. In: Lecture notes in computer science. Springer Verlag; 2014. p. 109–19.

[13] Basafa E, Sheikholeslami M, Mirbagheri A, Farahmand F, Vossoughi GR. Design and implementation of series elastic actuators for a haptic laparoscopic device. In: Proceedings of the 31st annual international conference of the IEEE engineering in medicine and biology society: engineering the future of biomedicine, EMBC 2009; 2009. p. 6054–7. doi:10.1109/IEMBS.2009.5332616. ISBN 9781424432967.

[14] Zinn M, Khatib O, Roth B, Salisbury JK. Large workspace haptic devices – a new actuation approach. In: Proceedings of symposium on haptics interfaces for virtual environment and teleoperator systems 2008; 2008. p. 185–92. doi:10.1109/HAPTICS.2008.4479941. ISBN 9781424420056.

[15] Oblak J, Matjačić Z. Design of a series visco-elastic actuator for multipurpose rehabilitation haptic device. J Neuroeng Rehabil 2011;8:3. doi:10.1186/1743-0003-8-3. http://www.pubmedcentral.nih.gov/articlerender.fcgi?artid=3063208&tool=pmcentrez&rendertype=abstract.

[16] Parietti F, Baud-Bovy G, Gatti E, Riener R, Guzzella L, Vallery H. Series viscoelastic actuators can match human force perception. IEEE/ASME Trans Mechatron 2011;16(5):853–60. doi:10.1109/TMECH.2011.2162076.

[17] Colgate E, Hogan N. An analysis of contact instability in terms of passive physical equivalents. In: Proceedings of IEEE international conference on robotics and automation, 1; 1989. p. 404–9. doi:10.1109/ROBOT.1989.100021.

[18] Van Der Schaft AJ. L2-gain and passivity techniques in nonlinear control. Lecture notes in control and information sciences, vol. 218. Springer-Verlag; 1996. ISBN 1852330732.

[19] Hogan N. Controlling impedance at the man/machine interface. In: Proceedings of international conference on robotics and automation. Scottsdale, AZ: IEEE Computer Society Press; 1989. p. 1626–31. doi:10.1109/ROBOT.1989.100210. ISBN 0-8186-1938-4.

[20] Vallery H, Veneman J, van Asseldonk EHF, Ekkelenkamp R, Buss M, van Der Kooij H. Compliant actuation of rehabilitation robots. IEEE Robot Autom Mag 2008;15(3):60–9. doi:10.1109/MRA.2008.927689. http://ieeexplore.ieee.org/lpdocs/epic03/wrapper.htm?arnumber=4624584.

[21] Pratt GA, Willisson P, Bolton C, Hofman A. Late motor processing in low-impedance robots: impedance control of series-elastic actuators. In: Proceedings of American control conference; 2004. p. 3245–51. http://ieeexplore.ieee.org/xpls/abs_all.jsp?arnumber=1384410.

[22] Oblak J, Matja Z. On stability and passivity of haptic devices characterized by a series elastic actuation and considerable end-point mass. In: Proceedings of IEEE international conference on rehabilitation robotics; 2011. p. 1–5. ETH Zurich Science City, ISBN 9781424498628.

[23] Albu-Schäffer A, Ott C, Hirzinger G. A unified passivity-based control framework for position, torque and impedance control of flexible joint robots. Int J Rob Res 2007;26(1):23–39. doi:10.1177/0278364907073776.

[24] Tagliamonte NL, Accoto D. Passivity constraints for the impedance control of series elastic actuators. J Syst Control Eng 2013;228(3):138–53.

[25] Boaventura T, Focchi M, Frigerio M, Buchli J, Semini C, Medrano-Cerda GA, et al. On the role of load motion compensation in high-performance force control. In: Proceedings of 2012 IEEE/RSJ international conference on intelligent robots and systems. IEEE; 2012. p. 4066–71. doi:10.1109/IROS.2012.6385953. ISBN 978-1-4673-1736-8.

[26] Wang M, Sun L, Yin W, Dong S, Liu J. A novel sliding mode control for series elastic actuator torque tracking with an extended disturbance observer. In: Proceedings of 2015 IEEE international conference on robotics and biomimetics (ROBIO); June 2015. p. 2407–12. doi:10.1109/ROBIO.2015.7419699.

[27] Yu H, Huang S, Chen G, Pan Y, Guo Z. Human–robot interaction control of rehabilitation robots with series elastic actuators. IEEE Trans Rob 2015;31(5):1089–100. doi:10.1109/TRO.2015.2457314.

[28] Oh S, Kong K. High precision robust force control of a series elastic actuator. IEEE/ASME Trans Mechatron 2016;4435(c):1. doi:10.1109/TMECH.2016.2614503. http://ieeexplore.ieee.org/document/7579567/.

[29] Calanca A, Fiorini P. Human-Adaptive control of series elastic actuators. Robotica 2014;2(08):1301–16. doi:10.1017/S0263574714001519.

[30] Kaya KD, Cetin L. Adaptive state feedback controller design for a rotary series elastic actuator. Trans Inst Meas Control 2017;39:61–74.

[31] dos Santos WM, Caurin GAP, Siqueira AAG. Design and control of an active knee orthosis driven by a rotary series elastic actuator. Control Eng Pract 2017;58:307–18.

[32] Calanca A, Capisani L, Fiorini P. Robust force control of series elastic actuators. Actuators 2014;3(3):182–204. Special issue on soft actuators doi: 10.3390/act3030182.

[33] Calanca A, Muradore R, Fiorini P. A review of algorithms for compliant control of stiff and fixed compliance robots. IEEE Tran Mechatron 2016;21(2):613–24. doi:10.1109/TMECH.2015.2465849.

[34] Brogliato B, Maschke B, Lozano R, Egeland O. Dissipative systems analysis and control: theory and applications. London: Springer-Verlag; 2007.

[35] Adams RJ, Hannaford B. Stable haptic interaction with virtual environments. IEEE Trans Rob 1999;15(3):465–74.

[36] Buerger S, Hogan N. Complementary stability and loop shaping for improved human-robot interaction. IEEE Trans Robot 2007;23(2):232–44. http://ieeexplore.ieee.org/xpls/abs_all.jsp?arnumber=4154828.

[37] Giovacchini F, Vannetti F, Fantozzi M, Cempini M, Cortese M, Parri A, Yan T, Lefeber D, Vitiello N. A light-weight active orthosis for hip movement assistance. Rob Auton Syst 2014.

[38] Sensinger JW, Weir RF. Improvements to series elastic actuators. In: Proceedings of IEEE/ASME international conference on mechatronic and embedded systems and applications; 2006. p. 1–7.

[39] Wyeth G. Demonstrating the safety and performance of a velocity sourced series elastic actuator. In: Proceedings of IEEE international conference of robotics and automation; 2008. p. 3642–7. ISBN 9781424416479

[40] Cannon RH, Rosenthal DE. Experiments in control of flexible structures with noncolocated sensors and actuators. J Guid Control 1984;3(3):546–53.

[41] Eppinger S, Seering W. Understanding bandwidth limitations in robot force control. In: Proceedings of 1987 IEEE international conference on robotics and automation, 4; 1987. p. 904–9. doi:10.1109/ROBOT.1987.1087932.

[42] Albu-Schäffer A, Hirzinger G. A globally stable state feedback controller for flexible joint robots. J Adv Robot 2001;15(8):799–814.

[43] Calanca A, Muradore R, Fiorini P. Impedance control of series elastic actuators using acceleration feedback. Cham: Springer International Publishing; 2017. p. 33–7. doi:10.1007/978-3-319-46532-6_6. ISBN 978-3-319-46532-6.

[44] Calanca A, Capisani LM, Ferrara A, Magnani L. MIMO Closed loop identification of an industrial robot. IEEE Trans Control Syst Technol 2011;19(5):1214–24. doi:10.1109/TCST.2010.2077294. http://ieeexplore.ieee.org/xpls/abs_all.jsp?arnumber=5634145.

Andrea Calanca received the Master degree in Computer Engineering cum laude from the University of Pavia in 2006. He worked in companies as Software, DSP and Control Engineer and in 2009 he joined the Altair Robotics Laboratory, University of Verona, where he received the Ph.D. in 2014 under the supervision of Prof. Paolo Fiorini. He is currently working at University of Verona as an Assistant Professor. His research interests are related to robotics, control and DSP with applications to rehabilitation robotics, physical human-robot interaction and assisted locomotion. He developed estimation and control algorithms for research and

market applications. He is the winner of a national prize from the Italian Industrial Robotic Society (SIRI) and the winner of a national makers competition organized by Elettronica Open Source.

Riccardo Muradore received the Laurea degree in Information Engineering in 1999 and the Ph.D. degree in Electronic and Information Engineering in 2003 both from the University of Padova (Italy). He held a post-doctoral fellowship at the Department of Chemical Engineering, Univ. of Padova, from 2003 to 2005. Then he spent three years at the European Southern Observatory in Munich (Germany) as Control Engineer working on adaptive optics systems. In 2008 he joined the ALTAIR robotics laboratory, University of Verona (Italy). Since 2013 he is an Assistant Professor. His research interests include robust control, teleoperation, robotics, networked control systems and adaptive optics.

Paolo Fiorini received the Laurea degree in Electronic Engineering from the University of Padova, (Italy), the MSEE from the University of California at Irvine (USA), and the Ph.D. in ME from UCLA (USA). From 1985 to 2000, he was with NASA Jet Propulsion Laboratory, California Institute of Technology, where he worked on telerobotic and teloperated systems for space exploration. From 2000 to 2009 he was an Associate Professor of Control Systems at the School of Science of the University of Verona (Italy) where he founded the ALTAIR robotics laboratory with his students. He is currently Full Professor of Computer Science at the University of Verona. His research focuses on teleoperation for surgery, service and exploration robotics funded by several European Projects. He is an IEEE Fellow (2009).